THE JOURNAL OF PHYSICAL CHEMISTRY C

Article

pubs.acs.org/JPCC

Organic–Inorganic Hybrid Lead Iodide Perovskite Featuring Zero Dipole Moment Guanidinium Cations: A Theoretical Analysis

Giacomo Giorgi,*[,†,‡] Jun-Ichi Fujisawa,[§,∥] Hiroshi Segawa,[§] and Koichi Yamashita*[,†,‡]

[†]Department of Chemical System Engineering, School of Engineering, The University of Tokyo, 7-3-1, Hongo, Bunkyo-ku, Tokyo 113-8656, Japan

[‡]CREST-JST, 7 Gobancho, Chiyoda-ku, Tokyo 102-0076, Japan

[§]Research Center for Advanced Science & Technology (RCAST), The University of Tokyo, 4-6-1, Komaba, Meguro-ku, Tokyo 153-8904, Japan

[∥]Japan Science & Technology Agency (JST), Precursory Research for Embryonic Science & Technology (PRESTO), 4-1-8, Honcho, Kawaguchi, Saitama 332-0012, Japan

ABSTRACT: Three-dimensional organic–inorganic lead iodide perovskites are potential photoconductive materials for solar cells. Nowadays, a high power conversion efficiency exceeding 20% can be achieved. However, perovskite solar cells are reported to suffer from a large hysteresis in the current–voltage curves. This may be attributed to the motion of organic cations with a permanent dipole moment in response to the applied electric field. Therefore, in order to suppress the hysteresis, organic cations that have a zero dipole moment and a molecular size well fitted to the lead iodide cavity are required. Using density functional theory calculations, we theoretically studied the thermodynamic stability and electronic properties of lead iodide perovskites with large guanidinium cations having a nearly zero dipole moment and compared the results with those predicted via the Goldschmidt tolerance factor. The properties of formamidinium–guanidinium ($FA_{1-x}GA_xPbI_3$) intermediate alloys were also investigated.

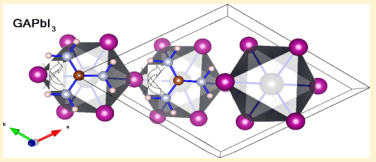

INTRODUCTION

Hybrid organic–inorganic lead iodide perovskites that consist of a three-dimensional (3D) lead iodide framework and organic counter cations are ambipolar photoconductive materials with potential for solar cell applications.[1−8] Recently, when employing the Cl-doped $MAPbI_3$ perovskite with methylammonium (MA; $[CH_3NH_3]^+$) cations, the power conversion efficiency of perovskite solar cells was increased up to 19.3% (Figure 1).[9]

However, perovskite solar cells suffer from a large hysteresis in the current–voltage curves.[10−12] Such hysteresis may originate from the motion of the MA cations with a large permanent dipole moment in the lead halide cavity. Therefore, in order to suppress the hysteresis, it is necessary to select organic cations that are well fitted to the lead iodide cavity and that have a zero dipole moment. Recently, Amat et al. theoretically examined the structure and electronic properties of the lead iodide perovskite ($FAPbI_3$) with larger formamidinium (FA; $[HC(NH_2)_2]^+$) cations (Figure 1) with a smaller dipole moment instead of MA cations.[13]

Theoretical approaches have been found to be very powerful predictive tools for exploring and "tailoring" new perovskites with desired properties.[14,15] Accordingly, in this study, we focused on the analysis of the slightly larger guanidinium (GA; $[C(NH_2)_3]^+$) cations (Figure 1), which have a nearly zero dipole moment.

The calculation of the dipole moment of a charged system is origin dependent; thus, in principle, a unique value cannot be determined. The comparison among different charged molecules is thus a function of the choice of a common system of coordinates for the species investigated. On the other hand, trends can be established for charged systems that share a common initial chemical skeleton (one example, $^+CH_3 \rightarrow {}^+CH_2X \rightarrow {}^+CHX_2 \rightarrow {}^+CX_3$, where X = halogen). In our case, several tests[16] have always given $\mu_{MA} \gg \mu_{FA} > \mu_{GA} \approx 0$, a result clearly related to the increasing symmetry of the three cations (MA < FA < GA).

Although, according to the empirical Goldschmidt tolerance factor, it is predicted that GA cations are slightly too large to be incorporated into the lead iodide cavity,[18,19] the stability and electronic properties of $GAPbI_3$ and of the intermediate alloys with formamidinium, $FA_{1-x}GA_xPbI_3$, deserve further attention. We theoretically examined the effects of the incorporation of GA cations into the lead iodide perovskite on the thermodynamic stability and electronic properties by means of density functional theory (DFT) calculations and in this paper discuss the results and compare them with those obtained applying the Goldschmidt tolerance factor. GA has already been studied in its combination with metal–organic frameworks,[20,21] and very interesting and unique chemical features have been found. This provides motivation for its investigation as an organic cation in materials for photovoltaic applications.

COMPUTATIONAL SETUP

Spin-polarized DFT calculations have been performed by means of the electron exchange-correlation functional proposed

Received: January 3, 2015
Published: February 5, 2015

DOI: 10.1021/acs.jpcc.5b00051
J. Phys. Chem. C 2015, 119, 4694−4701

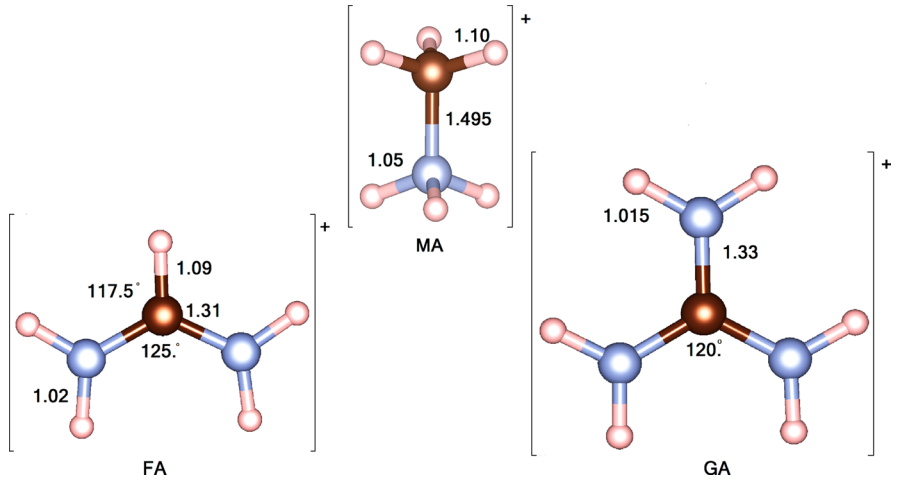

Figure 1. Optimized structures: (top) methylammonium (MA); (bottom, left) formadinium (FA); (bottom, right) guanidinium (GA) cations.[23−25] (Brown: carbon atom; blue: nitrogen atoms; white: hydrogen atoms.)

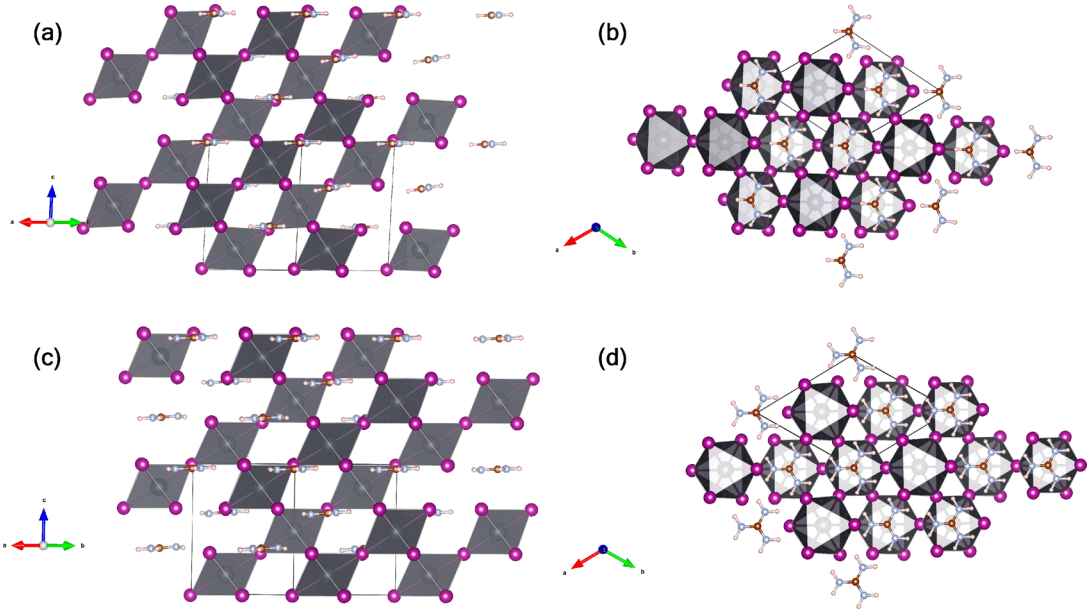

Figure 2. (a) Lateral view and (b) top view of the 2 × 2 × 2 optimized supercell of FAPbI3; (c) lateral view and (d) top view of the 2 × 2 × 2 optimized supercell of $GAPbI_3$. (Gray: lead atoms; purple: iodine atoms; brown: carbon atoms; blue: nitrogen atoms; white: hydrogen atoms.) Black solid line: unit cell.

by Perdew−Burke−Ernzerhof (PBE)[22] and also by means of its revised version for solids (PBESol)[23] as implemented in the VASP code,[24,25] with the main conclusions of our paper drawn on the basis of the latter approach. The projector augmented wave (PAW) method[26−28] has been similarly adopted.

In particular, we used a $5d^{10}6s^26p^2$ electron valence potential for the Pb atom. The cutoff energy for the plane-wave basis set was set to 500 eV. For the structural optimization, a 4 × 4 × 2 (6 × 6 × 4) Γ-centered *k*-point sampling of the Brillouin zone was used for the trigonal (tetragonal) structures considered, while 350 *k* points were used for the description of the electronic properties. Furthermore, spin orbit coupling (SOC) calculations were performed on the PAW/PBESol optimized structures, as the impact of relativistic effects on the electronic properties of hybrid organic−inorganic perovskites has been clearly demonstrated mainly in the conduction region.[5,29]

A charge analysis was performed by means of the Bader code,[30−32] increasing the fft grid of 25% with respect to the optimization grid default, in order to more accurately reproduce the correct total core charge.

RESULTS AND DISCUSSION

We first compared the stability of $GAPbI_3$ with that of $FAPbI_3$. The general lack of experimental data concerning $GAPbI_3$[33] makes the choice of the same unit cell for the two species the most reliable. In particular, we considered as a starting structure that reported by Stoumpos et al.[34] for the α phase of $FAPbI_3$ (trigonal, P_{3m1}, $Z = 3$) and fully optimized both ionic positions and lattice parameters for the two species. The unit cells of the two structures are reported in Figure 2, and Table 1 contains the main structural data of the two optimized structures.

To compare the absolute stability of the two mixed organic−inorganic halides, we calculated and then compared their formation energy from their cation and anion components.

As a reference for $[PbI_3]_3^{3-}$, we considered the same lattice geometry as in the optimized structures of both $FAPbI_3$ and

DOI: 10.1021/acs.jpcc.5b00051
J. Phys. Chem. C 2015, 119, 4694−4701

Table 1. Optimized Geometrical Parameters for the Structures of $FAPbI_3$ and $GAPbI_3$ Investigated Here (Lattice Parameters and Bond Lengths in Å, Angles in Degrees, Volumes in Å^3)

$FAPbI_3$	$GAPbI_3$
$a = b = 8.96$ [8.98[a]]	$a = b = 9.34$
$c = 10.63$ [11.00[a]]	$c = 10.33$
$\alpha = 87.7$	$\alpha = 89.6$
$\beta = 92.3$	$\beta = 90.4$
$\gamma = 116.6$	$\gamma = 119.4$
$d_{Pb-I\ ap} = 3.15-3.19$	$d_{Pb-I\ ap} = 3.18-3.23$
$d_{Pb-I\ eq} = 3.17-3.19$	$d_{Pb-I\ eq} = 3.18-3.25$
$d_{C-N} = 1.31$	$d_{C-N} = 1.33$
$V = 761.7$ (=820.53[b]) [768.9[a]]	$V = 786.1$ (=861.02[b])

[a]Reference 34. [b]PAW/PBE level.

$GAPbI_3$; we simply reoptimized the ionic positions after the cation removal (FA and GA, respectively). The ΔE_{form} was 0.22 eV per cation, with $FAPbI_3$ stabilized over $GAPbI_3$.

From the optimized crystalline structure of $FAPbI_3$, we similarly calculated the energy required to replace the three FA cations with three GA ones, that is, $E_{products} - E_{reactants}$ of the reaction

$$FAPbI_3 + GA \rightarrow GAPbI_3 + FA$$

The result was only 0.32 eV.

Considering the substitution of every single FA with a GA cation, one notices that the first FA replaced by GA is the thermodynamic bottleneck of the reaction, even if only costing 0.16 eV. The further two substitutions are almost energy free (both $\Delta E \sim 0.08$ eV). Details are as follows:

1) $FAPbI_3 + 1/3\ GA \rightarrow FA_{2/3}GA_{1/3}PbI_3 + 1/3\ FA$ $\Delta E_1 = 0.16$ eV

2) $FA_{2/3}GA_{1/3}PbI_3 + 1/3GA \rightarrow FA_{1/3}GA_{2/3}PbI_3 + 1/3FA$ $\Delta E_2 = 0.08$ eV

3) $FA_{1/3}GA_{2/3}PbI_3 + 1/3GA \rightarrow GAPbI_3 + 1/3FA$ $\Delta E_3 = 0.08$ eV

$\Delta E_{tot} = 0.32$ eV

Experimentally Szafrànski[33] has reported the preferential formation of low-dimensional structures for $GAPbI_3$. Such an experimental result is confirmed by our theoretical predictions. Anyway, no previous results concerning the alloys formed by $FAPbI_3$ and $GAPbI_3$ are reported in previous literature. Moving thus from the consistency obtained with the available reported experimental results for the 3D $GAPbI_3$,[33] we theoretically predict the stability of the $FA_{1-x}GA_xPbI_3$ intermediate alloys, describing in the following their electronic properties. Additionally, considering as chemical potential for $FAPbI_3$ and $GAPbI_3$ their PAW/PBESol calculated total energy per unit in the formation of the intermediate alloys, we obtain

1) $FAPbI_3 + 1/3\ GAPbI_3 \rightarrow FA_{2/3}GA_{1/3}PbI_3 + 1/3\ FAPbI_3$ $\Delta E_1 = 0.06$ eV

2) $FA_{2/3}GA_{1/3}PbI_3 + 1/3GAPbI_3 \rightarrow FA_{1/3}GA_{2/3}PbI_3 + 1/3FAPbI_3$ $\Delta E_2 = -0.03$ eV

3) $FA_{1/3}GA_{2/3}PbI_3 + 1/3GAPbI_3 \rightarrow GAPbI_3 + 1/3FAPbI_3$ $\Delta E_3 = -0.03$ eV

and similarly observe that processes 2 and 3 become energetically favored, further confirming the stability of the intermediate mixed alloys.

After considering the most stable structure of $GAPbI_3$, we checked for the possible presence of (meta)stable states. After rotating the plane of the GA molecule by 90° with respect to the most stable one, where the GA plane lies on the *ab* plane, we reoptimized our structures. In particular, we separately considered the rotation of one, two, and three GAs simultaneously.

Concerning the rotation of only one GA, we observed that, if we kept the lattice parameters and the semiconductor network atoms frozen, only allowing relaxation of the GA atom, the system evolved toward the initial one, with the three GAs lying on the *ab* plane (Figure 2c, d). Alternatively, if we still held frozen the lattice parameters optimized to the most stable structure, allowing optimization of *all* ions of both the GAs and the lead iodide network, we obtained a system where the GA was tilted by ~35° from the *c* axis and was more unstable by ~0.15 eV with respect to the initial system. Finally, once we had fully optimized the lattice parameters and ions of the whole system, we obtained the same energy, namely, 0.12 eV, which clearly relates this energy variation (~0.03 eV) to the semiconductor network rearrangement. This last-mentioned structure, $GAPbI_{3\text{-}1GA\_35°}$, is shown in Figure 3.

In the case of two GA cations initially rotated by 90° with respect to the original position, a metastable system was observed when a full optimization of lattice parameters and ionic positions was performed. Such a metastable state is accompanied by an additional energy of ~0.14 eV.

In the final case, where the initial structure is represented by the three GAs aligned along the *c* axis, we observed that the geometrical full optimization led to a system in which the GAs are slightly tilted with respect to the *c* axis ($GAPbI_{3\text{-}iso}$). This system, shown in Figure 4, is isoenergetic with the initial and most stable structure (see Figure 2c, d). Structurally, in $GAPbI_{3\text{-}iso}$, *a* and *b* are shorter and *c* is longer ($a = 8.73$ Å, $b =$

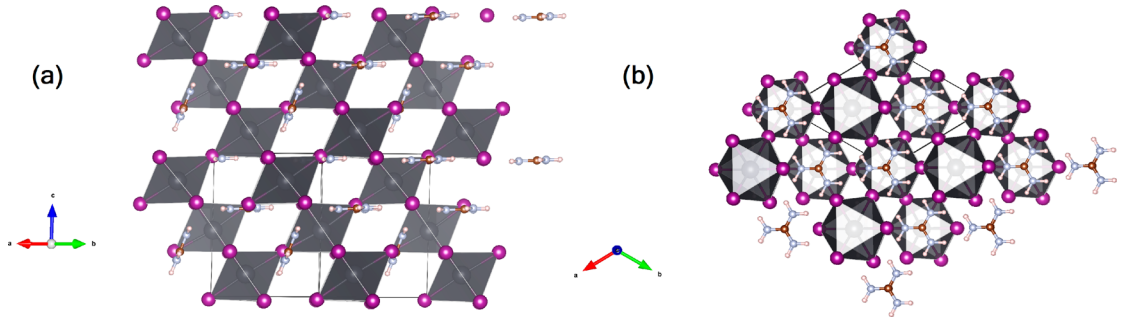

Figure 3. Supercell (2 × 2 × 2) of the optimized $GAPbI_{3\text{-}1GA\_35°}$ structure: (a) lateral view and (b) top view of the structure obtained by starting from one GA cation perpendicular to the ab plane. (Gray: lead atoms; purple: iodine atoms; brown: carbon atoms; blue: nitrogen atoms; white: hydrogen atoms.) Black solid line: unit cell.

DOI: 10.1021/acs.jpcc.5b00051
J. Phys. Chem. C 2015, 119, 4694−4701

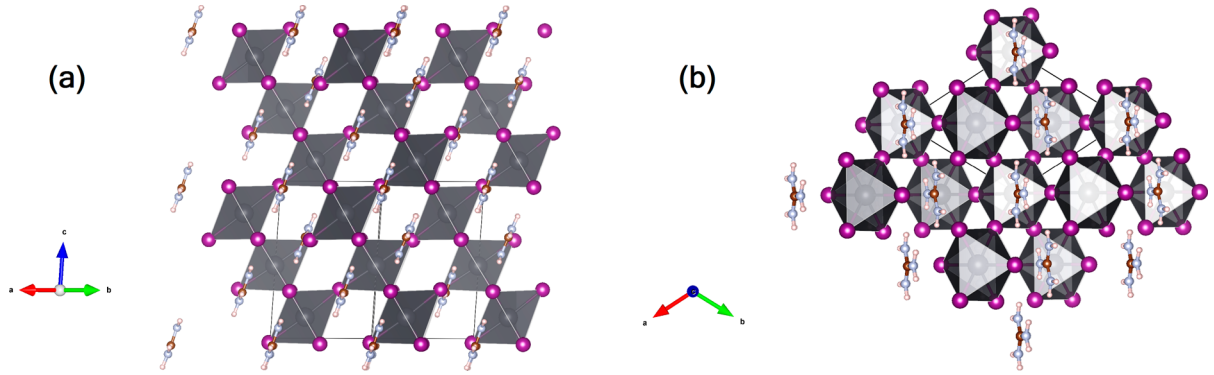

Figure 4. Supercell (2 × 2 × 2) of the optimized $GAPbI_{3\text{-}iso}$ structure: (a) lateral view and (b) top view of the structure obtained starting from the three GA cations perpendicular to the *ab* plane. (Gray: lead atoms; purple: iodine atoms; brown: carbon atoms; blue: nitrogen atoms; white: hydrogen atoms.) Black solid line: unit cell.

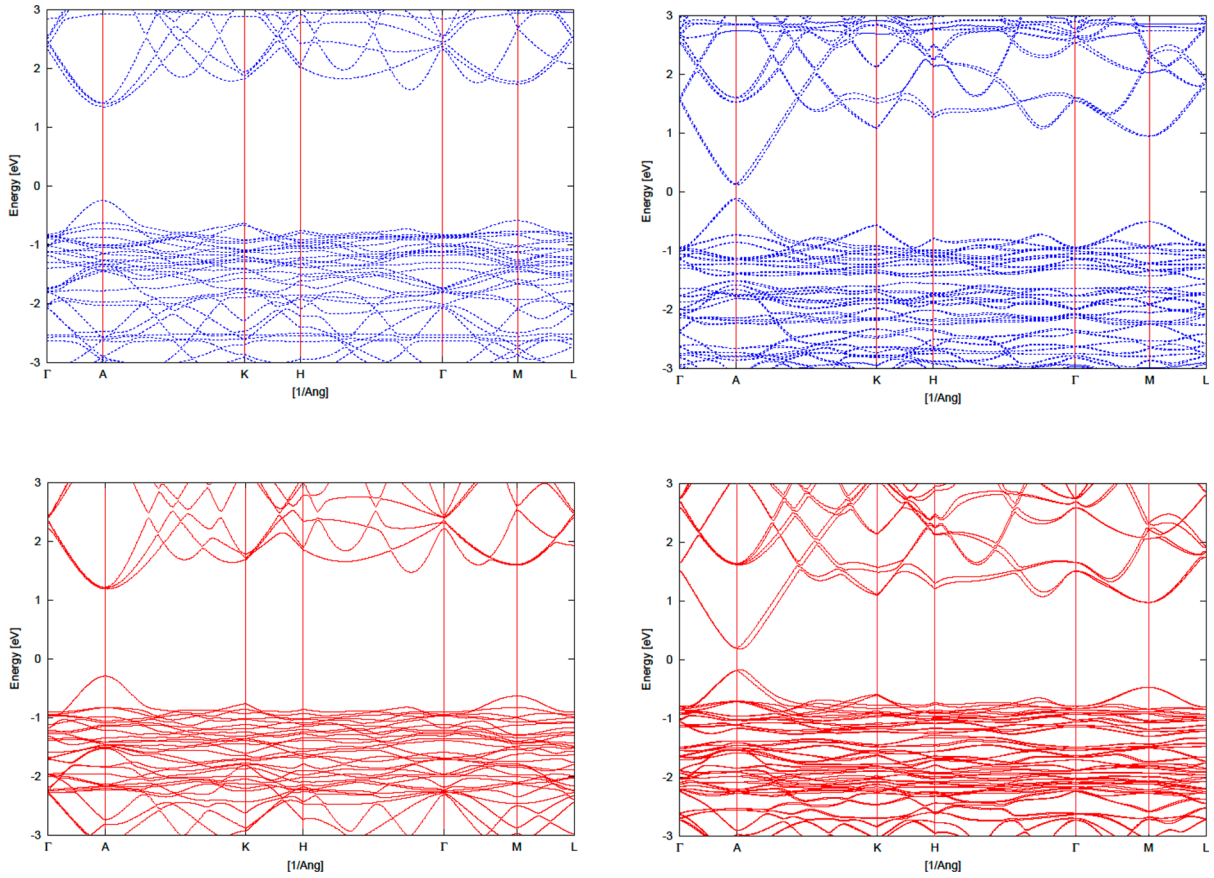

Figure 5. Top panel: band structure of $FAPbI_3$, calculated at (left) PBESol/PAW and (right) PBESol/PAW+SOC. Bottom panel: band structure of $GAPbI_3$, calculated at (left) PBESol/PAW and (right) PBESol/PAW+SOC. (Γ = 0.0, 0.0, 0.0; A = 0.0, 0.0, 0.5; K = 0.666, 0.333, 0.0; H = 0.666, 0.333, 0.5; M = 0.5, 0.0, 0.0; L = 0.5, 0.0, 0.5.) The zero corresponds to the Fermi energy of the systems.

8.76 Å, *c* = 11.39 Å) than those in the initially optimized $GAPbI_3$ system. However, of importance is that the final volume of the two systems is formally identical (786.1 $Å^3$ for $GAPbI_3$ vs 785.3 $Å^3$ for $GAPbI_{3\text{-}iso}$). Furthermore, the electronic properties are almost unaffected, as we will show later.

In Figure 5, $FAPbI_3$ and $GAPbI_3$ band structures are reported. Both systems are characterized by a direct bandgap on point A (0.0, 0.0, 0.5): 1.31 ($FAPbI_3$) and 1.49 eV ($GAPbI_3$), respectively. Concerning the former system, the bandgap that we found is slightly smaller than the value reported by Amat et al.[13] This difference stems from the different exchange-correlation potential employed. The underestimation of the bandgap associated with the PBESol is a feature that has been observed previously.[35] The same bandgap calculated for $FAPbI_3$ ($GAPbI_3$) and optimized at the PAW/PBE level is 1.57 eV (1.78 eV), which is in fair agreement with previously reported values.[13]

Most importantly, once we included the relativistic effects (SOC) in the calculations, consistency was found regarding the variation in the bandgap. In particular, we predicted bandgaps at PBESol+SOC that were 0.23 and 0.35 eV for $FAPbI_3$ and $GAPbI_3$, respectively, on some point close to A along the A → K direction. The difference in the bandgap is thus ∼1.1 eV, which is in fair agreement with what is reported in the paper of

DOI: 10.1021/acs.jpcc.5b00051
J. Phys. Chem. C 2015, 119, 4694−4701

Amat et al.[13] and also with other previously reported results for similar systems.[6,29] Furthermore, the increased value of the bandgap on A for $GAPbI_3$ is consistent with the fact that a more bulky cation (GA > FA) reduces the antibonding interactions between Pb and I orbitals forming the valence band maximum (VBM) and the conduction band minimum (CBM) of similar systems. In other words, the VBM (and to a lesser extent the CBM, where the presence of I orbitals is negligible) will be stabilized, with a subsequent bandgap opening. The inclusion of relativistic effects induces the splitting (Dresselhaus spin−orbit effect) of the band edges mainly marked along the A → K direction. This is a well-known effect that has been reported for similar systems.[8]

We calculated the photocarrier effective masses for both $FAPbI_3$ and $GAPbI_3$ at the PBESol level finding that, along the A−Γ direction, $m_h^* = 0.302m_0$ and $m_e^* = 0.403m_0$ for the former, and $m_h^* = 0.385m_0$ and $m_e^* = 0.359m_0$ for the latter. The ratio between m_h^* and m_e^*, 0.75 for $FAPbI_3$ and 1.07 for $GAPbI_3$, qualitatively indicates that, at this level, $GAPbI_3$ has a more marked ambipolar behavior than $FAPbI_3$, which at variance, seems to be preferable as a hole transport material. We are aware of the shortcomings of DFT in the description of the conduction region. Nevertheless, we are confident of the reliability of our results, as the ambipolarity of this class of materials is both reported at the experimental level[1−4] and confirmed by means of a more accurate level of theory based on Green's function.[8,36]

For the sake of completeness, in Figure 6, we report the band structure of $GAPbI_{3\text{-}iso}$, the structure of which is given in Figure 3. The bandgap on point A is formally identical to that of the initially optimized system (~1.47 eV).

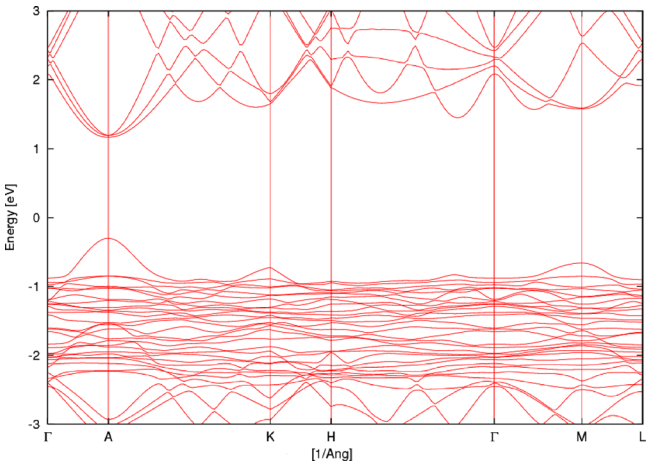

Figure 6. Band structure of $GAPbI_{3\text{-}iso}$ calculated at PBESol/PAW. (Γ = 0.0, 0.0, 0.0; A = 0.0, 0.0, 0.5; K = 0.666, 0.333, 0.0; H = 0.666, 0.333, 0.5; M = 0.5, 0.0, 0.0; L = 0.5, 0.0, 0.5.) The zero corresponds to the Fermi energy of the system.

In Figure 7, we report the $GAPbI_3$ wave function at point A for the VBM and for the CBM. The VBM, as in most organic−inorganic halide perovskites, is mainly constituted by the antibonding combination of Pb 6s orbitals and I 5p orbitals while the CBM is constituted by the antibonding combination of Pb 6p orbitals with traces of I 5s orbitals.

Then, we calculated the bandgaps for the two intermediate species $FA_{2/3}GA_{1/3}PbI_3$ and $FA_{1/3}GA_{2/3}PbI_3$ and found that, on point A, the gap at PBESol (PBESol+SOC) for the former is 1.42 eV (0.34 eV) and for the latter is 1.47 eV (0.39 eV). The two intermediate alloys show an anomalous bowing behavior with their gaps resulting to be more productlike, that is, closer to that of $GAPbI_3$. In details, replacing the first FA with only one GA induces a noticeable bandgap opening of ~8.5% compared with the parental $FAPbI_3$, and the final $GAPbI_3$ shows a bandgap opening of 13.8% compared with the $FAPbI_3$. The inclusion of relativistic effects, drastically reducing the bandgap values, clearly amplifies this trend by a factor of 4 (8.5% → 36%).

Although they are characterized by different crystalline symmetry, an interesting comparison is that between the electronic properties of the two trigonal species $FAPbI_3$ and $GAPbI_3$ and those of tetragonal *t*-$MAPbI_3$. For the latter species, we fully optimized the lattice parameter and ionic positions. We began with the experimental structure reported by Kawamura et al.[37] and obtained a structure close to the "*head-to-tail*" structure reported by Mosconi et al.[38] for *t*-$MAPbI_3$, with $a = b = 8.70$ Å and $c = 12.82$ Å. Similar to the previous cases investigated here, the PAW/PBESol calculated bandgap (Γ, 1.40 eV) is slightly underestimated with respect to the PAW/PBE one (Γ, 1.59 eV).

We thus normalized the orbital contributions and compared the band edges for the three systems (Figure 8). We found that,

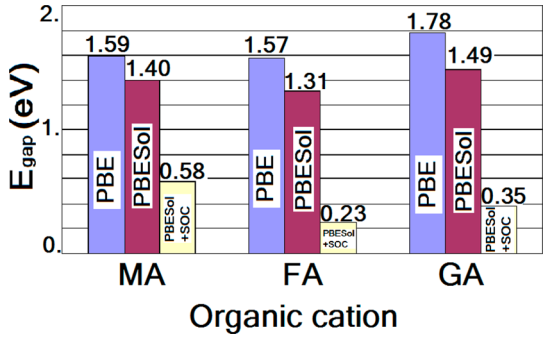

Figure 8. Bandgap for the three systems $XPbI_3$ (X = MA, FA, GA) at PBE (purple), PBESol (magenta), and PBESol+SOC (yellow). The bandgap is direct on Γ (0.0, 0.0, 0.0) for MA at all levels of calculation and on A (0.0, 0.0, 0.5) for FA and GA at the PBE and PBESol levels. For the latter two at PBESol+SOC, the minimum bandgap is at some point close to A.

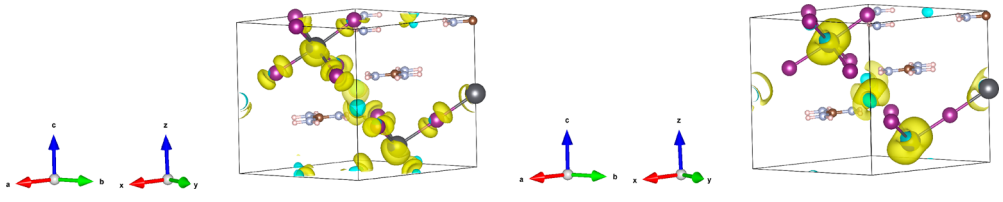

Figure 7. $GAPbI_3$: (left) CBM; (right) VBM. Wave functions calculated at the Γ point at the PAW/PBESol level (isosurface level, 6e-04).

DOI: 10.1021/acs.jpcc.5b00051
J. Phys. Chem. C 2015, 119, 4694−4701

for *t*-$MAPbI_3$, the VBM on Γ is the antibonding combination of the Pb 6s (32.7%) and the I 5p orbitals (66.6% = 25.7% $5p_y$ + 15.2% $5p_z$ + 25.7% $5p_x$), and the CBM, still on Γ, is mainly constituted by the Pb 6p orbital (80% $6p_z$) in an antibonding fashion with traces of other I orbitals.

When considering the two trigonal structures, a noticeable change in the band edges population can be observed. Whereas the VBM (on A) for both $FAPbI_3$ and $GAPbI_3$ remains very similar to that of *t*-$MAPbI_3$ (on Γ), the nature of the CBM is quite different. In *t*-$MAPbI_3$, it is mainly localized only along the Pb $6p_z$ orbitals whereas, in the latter case (FA, GA), it is more delocalized along the three directions of the Pb p orbitals (49.8% $6p_y$ + 14.0% $6p_z$ + 16.7% $6p_x$ for $FAPbI_3$; 3.7% $6p_y$ + 70.2% $6p_z$ + 8.4% $6p_x$ for $GAPbI_3$). This delocalization induces the CBM stabilization. In the case of $GAPbI_3$, the wider bandgap stems from the combination of this effect and the presence of the more bulky organic cation GA that, as previously reported,[6] tends to reduce the antibonding interaction at the VBM and stabilizes it, with a subsequent opening of the gap.

As mentioned previously, the PBESol exchange-correlation functional results in an underestimated description of the bandgaps compared with the PBE calculated ones. Then, we included relativistic effects on the PBESol optimized structure (single-point calculation), and similarly, we also fully reoptimized the structures at the PBESol+SOC level. As also previously reported,[39] the impact of SOC on the structural properties of these materials is only marginal. As a consequence, the two procedures lead to almost identical results concerning the bandgaps for the three systems studied. Noticeably, an *up*−*down*−*up* trend is present at each level of calculation in the MA → FA → GA series. Overall, the inclusion of relativistic effects results in the interesting enhanced reduction of the bandgap for $GAPbI_3$ compared with $MAPbI_3$.

Spinors at the PBESol+SOC level result in very similar composition for the three cases. We may therefore ascribe the more marked correction induced by relativistic effects on $FAPbI_3$ and $GAPbI_3$ to the change in symmetry from tetragonal ($MAPbI_3$) to trigonal.

As reported by Brivio et al.,[35] calculations for cubic (*c*-) $MAPbI_3$ show bandgaps that are 1.4 eV at the PBESol level and 2.0 eV at the HSE06 level, respectively. Similarly, we have previously shown that the combination of a nonlocal hybrid functional, that is, HSE06, and of relativistic effects does not satisfactorily reproduce the experimental data, still leading to a non-negligible underestimation of the true bandgap.[6]

In this context, many body perturbation theory, in the framework of the *GW* method[8,36] combined with relativistic effects, offers a solid and extremely valuable tool to bypass the bandgap underestimation given by the pure DFT+SOC scheme. Very satisfactory results have been reported by Brivio et al.[8] and Umari et al.[36] In the latter case, for example, close agreement is found between the *GW*+SOC calculated bandgaps of *t*-$MASnI_3$ and *t*-$MAPbI_3$ (1.10 and 1.67 eV, respectively) and the experimental values for the same systems (1.20 and 1.60 eV, respectively). Similarly, the inclusion of relativistic effects is found to be fundamental at each level of calculation mainly for $MAPbI_3$. At variance, the $MASnI_3$ bandgap results are less affected by their inclusion ($MASnI_3$: 0.61 eV (scalar relativistic (SR)-DFT); 1.55 eV (SR-*GW*); 0.31 eV (SOC-DFT); 1.10 eV (SOC-*GW*); 1.20 (expt). $MAPbI_3$: 1.68 eV (SR-DFT); 2.68 eV (SR-*GW*); 0.60 eV (SOC-DFT); 1.67 eV (SOC-*GW*); 1.60 (expt)).[36]

We are thus aware that a *GW*+SOC treatment could be beneficial for the description of the electronic properties of the present investigated systems, that is, $FAPbI_3$, $GAPbI_3$, and their intermediate alloys; at the same time, here, we clearly aim at first to discuss their stability in terms of thermodynamic properties. In this sense, even if clearly biased by the DFT systematic underestimation of the bandgap, we still consider the initial comparison of the PBE, PBESol, and PBESol+SOC calculated bandgaps to be extremely meaningful, addressing further refinements of their values, at higher levels of calculation, to future investigations.

As free cations, FA and GA are Lewis acids, with the latter stronger than the former. This is a consequence of the presence of electronegative N atoms surrounding the central C atom that subtract charge from it. A feature that deserves attention here is the charge distribution in the two cations FA and GA and the role that the interaction with the inorganic semiconductor plays in this distribution. Thus, we performed a Bader charge analysis[30−32] of the cations, in both a free and a semiconductor-embedded environment.

In the case of FA, we observed that the difference (δq) between the charges on C and N in the free cation is 3.59*e*. This δq value ranges from 3.37*e* to 3.45*e* when FA is surrounded by the inorganic network, meaning that, in the latter case, the C−N bond is more covalent than in the free case.

In the case of GA, at variance, δq between C and N charges is larger in the case of the ion embedded in the semiconductor (average $\delta q \sim 4.26e$) than in the free case where $\delta q \sim 3.99e$. This reveals a different interaction between the organic and the inorganic parts of the perovskite induced by the replacement of the aliphatic H atom with the third NH_2 group.

Thus, the presence of the third NH_2 group has a significant impact on both the structural and electronic properties of the final hybrid organic−inorganic halide perovskite. Clearly, it increases the number of H bonds occurring between the partly negatively charged (δ^-) I atoms and partly positively charged (δ^+) ammonium H atoms.[33] This result has the nontrivial consequence of increasing the shrinkage of the final cell.

A simple yet useful procedure to compare the shrinkage induced by cations involves calculating the ratio between the volume of the unit cells of $FAPbI_3$ and $GAPbI_3$ (see Table 1) and three times (P_{3m1}, $Z = 3$) the volume of the corresponding cation (FA = 84.152 Å^3; GA = 102.182 Å^3).[40] A constant value would indeed indicate no impact of the cation on the shrinkage of the final cell. We actually obtained 3.02 for $FAPbI_3$/3FA and 2.56 for $GAPbI_3$/3GA (3.25 and 2.80 at the PBE level of calculation), indicating an evident contraction of a $GAPbI_3$ cell induced by the increased number of semiconductor barrier[41] Coulomb interactions. Such a trend was confirmed after calculating the volumes from the atomic radii (r_{Aeff}) previously reported[19] (FA = 2.53 Å; GA = 2.78 Å), obtained according to the following formula:

$$r_{Aeff} = r_{mass} + r_{ion}$$

where r_{mass} represents the distance between the center of the mass of the molecule and the atom with the largest distance to the center of the mass, excluding H atoms, and r_{ion} is the corresponding ionic radius of this atom obtained from previous experimental reports.[42] In this case, the ratios are 3.74 for

DOI: 10.1021/acs.jpcc.5b00051
J. Phys. Chem. C 2015, 119, 4694−4701

$FAPbI_3$/3FA and 2.91 for $GAPbI_3$/3GA, indicating greater shrinkage of the latter over the former.

This result shows that other factors, in addition to that fundamental of the tolerance,[18,19] must be taken into account when predicting the existence of hybrid organic−inorganic perovskites.

CONCLUSIONS

In the context of hybrid organic−inorganic perovskite systems with applicability in photovoltaics, we have theoretically characterized the guanidinium lead iodide system, $GAPbI_3$, and the intermediate alloys it forms with formamidinium, $FA_{1-x}GA_xPbI_3$. We have compared its structural and electronic properties with those of other already well-known and characterized hybrid organic−inorganic perovskite systems.

Its thermodynamic stability, low formation energy, and bandgap make $GAPbI_3$ a potential candidate for future photovoltaic applications.

The introduction of a third NH_2 group results in very interesting and useful features in the final perovskite, which is expected to frustrate the more bulky GA cation rotation in the semiconductor cavity. Furthermore, and most importantly, inducing a zero dipole moment, associated with the D_{3h} symmetry of the GA cation, confers on $GAPbI_3$ the property of potentially reducing the experimentally reported hysteresis of the current−voltage curve previously observed for smaller cations such as MA and ascribed to rotation triggering light plus bias conditions.

AUTHOR INFORMATION

Corresponding Authors

*(G.G.) E-mail: giacomo@tcl.t.u-tokyo.ac.jp.

*(K.Y.) E-mail: yamasita@chemsys.tcl.t.u-tokyo.ac.jp.

Notes

The authors declare no competing financial interest.

ACKNOWLEDGMENTS

G.G. wants to thanks Dr. F. De Angelis of the Computational Laboratory for Hybrid/Organic Photovoltaics (CLHYO), CNR-ISTM of Perugia (ITALY), and Dr. V. Gonzalez-Pedro of the Departament de Física, Universitat Jaume I Castelló (SPAIN) for the always fruitful and stimulating scientific discussions.

REFERENCES

(1) Liu, M.; Johnston, M. B.; Snaith, H. J. Efficient Planar Heterojunction Perovskite Solar Cells by Vapour Deposition. *Nature* **2013**, *501*, 395−398.

(2) Burschka, J.; Pellet, N.; Moon, S.-J.; Humphry-Baker, R.; Gao, P.; Nazeeruddin, M. K.; Grätzel, M. Sequential Deposition as a Route to High-Performance Perovskite-Sensitized Solar Cells. *Nature* **2013**, *499*, 316−319.

(3) Stranks, S. D.; Eperon, G. E.; Grancini, G.; Menelaou, C.; Alcocer, M. J. P.; Leijtens, T.; Herz, L. M.; Petrozza, A.; Snaith, H. J. Electron-Hole Diffusion Lengths Exceeding 1 Micrometer in an Organometal Trihalide Perovskite Absorber. *Science* **2013**, *342*, 341−344.

(4) Xing, G.; Mathews, N.; Sun, S.; Lim, S. S.; Lam, Y. M.; Grätzel, M.; Mhaisalkar, S.; Sum, T. C. Long-Range Balanced Electron- and Hole-Transport Lengths in Organic-Inorganic $CH_3NH_3PbI_3$. *Science* **2013**, *342*, 344−347.

(5) Giorgi, G.; Fujisawa, J.-I.; Segawa, H.; Yamashita, K. Small Photocarrier Effective Masses Featuring Ambipolar Transport in Methylammonium Lead Iodide Perovskite: A Density Functional Analysis. *J. Phys. Chem. Lett.* **2013**, *4*, 4213−4216.

(6) Giorgi, G.; Fujisawa, J.-I.; Segawa, H.; Yamashita, K. Cation Role in Structural and Electronic Properties of 3D Organic−Inorganic Halide Perovskites: A DFT Analysis. *J. Phys. Chem. C* **2014**, *118*, 12176−12183.

(7) Giorgi, G.; Yamashita, K. Organic−Inorganic Halide Perovskites: An Ambipolar Class of Materials with Enhanced Photovoltaic Performances. *J. Mater. Chem. A* [Online early access]. DOI: 10.1039/C4TA05046K. Published Online: Nov 5, **2014**. http://pubs.rsc.org/en/content/articlelanding/2014/ta/c4ta05046k#!divAbstract.

(8) Brivio, F.; Butler, K. T.; Walsh, A.; van Schilfgaarde, M. Relativistic Quasiparticle Self-Consistent Electronic Structure of Hybrid Halide Perovskite Photovoltaic Absorbers. *Phys. Rev. B* **2014**, *89*, 155204 1−6.

(9) Zhou, H.; Chen, Q.; Li, G.; Luo, S.; Song, T.; Duan, H.-S.; Hong, Z.; You, J.; Liu, Y.; Yang, Y. Interface Engineering of Highly Efficient Perovskite Solar Cells. *Science* **2014**, *345*, 542−546.

(10) Snaith, H. J.; Abate, A.; Ball, J. M.; Eperon, G. E.; Leijtens, T.; Noel, N. K.; Stranks, S. D.; Wang, J. T.-W.; Wojciechowski, K.; Zhang, W. Anomalous Hysteresis in Perovskite Solar Cells. *J. Phys. Chem. Lett.* **2014**, *5*, 1511−1515.

(11) Gottesman, R.; Haltzi, E.; Gouda, L.; Tirosh, S.; Bouhadana, Y.; Zaban, A.; Mosconi, E.; De Angelis, F. Extremely Slow Photoconductivity Response of $CH_3NH_3PbI_3$ Perovskites Suggesting Structural Changes under Working Conditions. *J. Phys. Chem. Lett.* **2014**, *5*, 2662−2669.

(12) Sanchez, R. S.; Gonzalez-Pedro, V.; Lee, J.-W.; Park, N.-G.; Kang, Y. S.; Mora-Sero, I.; Bisquert, J. Slow Dynamic Processes in Lead Halide Perovskite Solar Cells. Characteristic Times and Hysteresis. *J. Phys. Chem. Lett.* **2014**, *5*, 2357−2363.

(13) Amat, A.; Mosconi, E.; Ronca, E.; Quarti, C.; Umari, P.; Nazeeruddin, Md. K.; Grätzel, M.; De Angelis, F. Cation-Induced Band-Gap Tuning in Organohalide Perovskites: Interplay of Spin−Orbit Coupling and Octahedra Tilting. *Nano Lett.* **2014**, *14*, 3608−3616.

(14) Castelli, I. E.; Olsen, T.; Datta, S.; Landis, D. D.; Dahl, S.; Thygesen, K. S.; Jacobsen, K. W. Computational Screening of Perovskite Metal Oxides for Optimal Solar Light Capture. *Energy Environ. Sci.* **2012**, *5*, 5814−5819.

(15) Castelli, I. E.; García-Lastra, J. M.; Thygesen, K. S.; Jacobsen, K. W. Bandgap Calculations and Trends of Organometal Halide Perovskites. *APL Mater.* **2014**, *2*, 081514 1−7.

(16) The dipole moment is calculated with the Gaussian09 package[17] at the rb3lyp/6-31+g(d,p) level of calculations.

(17) Frisch, M. J.; Trucks, G. W.; Schlegel, H. B.; Scuseria, G. E.; Robb, M. A.; Cheeseman, J. R.; Scalmani, G.; Barone, V.; Mennucci, B.; Petersson, G. A.; et al. *Gaussian 09*, Revision A.02; Gaussian, Inc.: Wallingford, CT, 2009.

(18) Goldschmidt, V. M. Die Gesetze der Krystallochemie. *Naturwissenschaften* **1926**, *14*, 477−485.

(19) Kieslich, G.; Sun, S.; Cheetham, A. K. Solid-State Principles Applied to Organic−Inorganic Perovskites: New Tricks for an Old Dog. *Chem. Sci.* **2014**, *5*, 4712−4715.

(20) Li, W.; Thirumurugan, A.; Barton, P. T.; Lin, Z.; Henke, S.; Yeung, H. H.-M.; Wharmby, M. T.; Bithell, E. G.; Howard, C. J.; Cheetham, A. K. Mechanical Tunability via Hydrogen Bonding in Metal−Organic Frameworks with the Perovskite Architecture. *J. Am. Chem. Soc.* **2014**, *136*, 7801−7804.

(21) Stroppa, A.; Barone, P.; Jain, P.; Perez-Mato, J.-M.; S. Picozzi, S. Hybrid Improper Ferroelectricity in a Multiferroic and Magnetoelectric Metal-Organic Framework. *Adv. Mater.* **2013**, *25*, 2284−2290.

(22) Perdew, J. P.; Burke, K.; Ernzerhof, M. Generalized Gradient Approximation Made Simple. *Phys. Rev. Lett.* **1996**, *77*, 3865−3868.

(23) Perdew, J. P.; Ruzsinszky, A.; Csonka, G. I.; Vydrov, O. A.; Scuseria, G. E.; Constantin, L. A.; Zhou, X.; Burke, K. Restoring the Density-Gradient Expansion for Exchange in Solids and Surfaces. *Phys. Rev. Lett.* **2008**, *100*, 136406 1−4.

DOI: 10.1021/acs.jpcc.5b00051
J. Phys. Chem. C 2015, 119, 4694−4701

(24) Kresse, G.; Furthmüller, J. Efficiency of ab-Initio Total Energy Calculations for Metals and Semiconductors Using a Plane-Wave Basis Set. *Comput. Mater. Sci.* **1996**, *6*, 15−50.
(25) Kresse, G.; Furthmüller, J. Efficient Iterative Schemes for *ab Initio* Total-Energy Calculations Using a Plane-Wave Basis Set. *Phys. Rev. B* **1996**, *54*, 11169−11186.
(26) Blöchl, P. E. Projector Augmented-Wave Method. *Phys. Rev. B* **1994**, *50*, 17953−17979.
(27) Kresse, G.; Joubert, D. From Ultrasoft Pseudopotentials to the Projector Augmented-Wave Method. *Phys. Rev. B* **1999**, *59*, 1758−1775.
(28) Blöchl, P. E.; Först, C. J.; Schimpl, J. Projector Augmented Wave Method: *Ab Initio* Molecular Dynamics with Full Wave Functions. *Bull. Mater. Sci.* **2003**, *26*, 33−41.
(29) Even, J.; Pedesseau, L.; Jancu, J.-M.; Katan, C. Importance of Spin−Orbit Coupling in Hybrid Organic/Inorganic Perovskites for Photovoltaic Applications. *J. Phys. Chem. Lett.* **2013**, *4*, 2999−3005.
(30) Tang, W.; Sanville, E.; Henkelman, G. A Grid-Based Bader Analysis Algorithm without Lattice Bias. *J. Phys.: Condens. Matter* **2009**, *21*, 084204 1−7.
(31) Sanville, E.; Kenny, S. D.; Smith, R.; Henkelman, G. Improved Grid-Based Algorithm for Bader Charge Allocation. *J. Comput. Chem.* **2007**, *28*, 899−908.
(32) Henkelman, G.; Arnaldsson, A.; Jónsson, H. A Fast and Robust Algorithm for Bader Decomposition of Charge Density. *Comput. Mater. Sci.* **2006**, *36*, 354−360.
(33) Szafrànski, M. Investigation of Phase Instabilities in Guanidinium Halogenoplumbates(II). *Thermochim. Acta* **1997**, *307*, 177−183.
(34) Stoumpos, C. C.; Malliakas, C. D.; Kanatzidis, M. G. Semiconducting Tin and Lead Iodide Perovskites with Organic Cations: Phase Transitions, High Mobilities, and Near-Infrared Photoluminescent Properties. *Inorg. Chem.* **2013**, *52*, 9019−9038.
(35) Brivio, F.; Walker, A. B.; Walsh, A. Structural and Electronic Properties of Hybrid Perovskites for High-Efficiency Thin-Film Photovoltaics from First-Principles. *APL Mater.* **2013**, *1*, 042111 1−4.
(36) Umari, P.; Mosconi, E.; De Angelis, F. Relativistic GW Calculations on $CH_3NH_3PbI_3$ and $CH_3NH_3SnI_3$ Perovskites for Solar Cell Applications. *Sci. Rep.* **2014**, *4*, 4467 1−7.
(37) Kawamura, Y.; Mashiyama, H.; Hasebe, K. Structural Study on Cubic−Tetragonal Transition of $CH_3NH_3PbI_3$. *J. Phys. Soc. Jpn.* **2002**, *71*, 1694−1697.
(38) Mosconi, E.; Amat, A.; Nazeeruddin, Md. K.; Grätzel, M.; De Angelis, F. First-Principles Modeling of Mixed Halide Organometal Perovskites for Photovoltaic Applications. *J. Phys. Chem. C* **2013**, *117*, 13902−13913.
(39) Egger, D. A.; Kronik, L. Role of Dispersive Interactions in Determining Structural Properties of Organic−Inorganic Halide Perovskites: Insights from First-Principles Calculations. *J. Phys. Chem. Lett.* **2014**, *5*, 2728−2733.
(40) Volumes of the cavities are calculated with Gaussian09[17] at the rb3lyp/6-31+g(d,p) level by means of the polarizable continuum model (PCM).
(41) Papavassiliou, G. C. Three- and Low-Dimensional Inorganic Semiconductors. *Prog. Solid State Chem.* **1997**, *25*, 125−270.
(42) Glazer, A. M. The Classification of Tilted Octahedra in Perovskites. *Acta Crystallogr.* **1972**, *B28*, 3384−3392.

DOI: 10.1021/acs.jpcc.5b00051
J. Phys. Chem. C 2015, 119, 4694−4701